# Influence of the Free Compression Stage on Magnetic Pulse Welding of Tubes

**J. Lueg-Althoff[1*], B. Schilling[1], J. Bellmann[2,3], S. Gies[1], S. Schulze[3], A. E. Tekkaya[1], E. Beyer[2,3]**

[1] Institute of Forming Technology and Lightweight Components, TU Dortmund University, Germany
[2] Institute of Manufacturing Technology, TU Dresden University, Germany
[3] Fraunhofer Institute for Material and Beam Technology IWS, Dresden, Germany
*Corresponding author. Email: Joern.Lueg-Althoff@iul.tu-dortmund.de

## Abstract

*In magnetic pulse welding (MPW) of tubular parts, the acceleration of the 'flyer' part typically corresponds to a free electromagnetic compression (EMC) process over the distance of the initial standoff between the outer and inner tube. During this process stage, already significant plastic strains occur. In addition, wrinkling is a phenomenon frequently observed during EMC. In this manuscript, influencing factors on the wrinkling effect are identified, taking the initial geometry of the flyer tube and its manufacturing process into account. Moreover, a link between the strains and wrinkles caused by the tube compression and the MPW process is made.*

*An experimental study is performed aiming for the quantification of the plastic deformation during EMC. The effect of this deformation on the stability and adhesion of brittle surface layers is analyzed. Accompanying numerical simulations help to understand the wrinkle formation and its influencing factors. Based on the results, hints for an improved process design of MPW are given.*

## Keywords

Joining, Welding, Magnetic Pulse Welding

# 1 Introduction

Most technical structures consist of more than one part, which makes joining processes key steps in manufacturing chains. For the implementation of lightweight concepts, the choice of the best material for every single component of a structure is pursued. For example, only highly stressed parts are made of steel, while parts without important structural functions are made of lower strength and lower density materials like aluminum. This increases the demand of joining dissimilar materials. Solid state impact welding processes like magnetic pulse welding (MPW) are especially suitable for this requirement. Since the heat input is limited, errors, which are typically related to fusion welding, can be minimized or completely be avoided (Mori et al., 2013).

In this process, the two tubular joining partners are positioned coaxially with some standoff $a$ in the working area of a tool coil, see **Fig. 1b**. When the electric energy $E$ stored in a capacitor bank is discharged via the coil in a damped sinusoidal current $I(t)$, eddy currents form in the 'flyer' part, which therefore must have a good electric conductivity. Lorentz forces, which can be represented by the magnetic pressure $p_m(t)$, cause the flyer's rapid acceleration towards the other joining partner. After a free forming stage, the collision with the inner ('parent') part must be oblique and with a certain impact velocity $v_{i,r}$ (**Fig. 1a**). If this is ensured, a material flow called 'jet' is formed, which is regarded as a prerequisite for the welding effect under high impact pressures $p_i$. The resulting weld seams are usually stronger than the weaker base material and often show a characteristic wavy appearance at the interface (**Fig. 1c**). Typically, the MPW process is designed in a way that the first impact takes place at the flyer end. This ensures the formation of a single weld front by adjusting the working length (Lorenz et al., 2016).

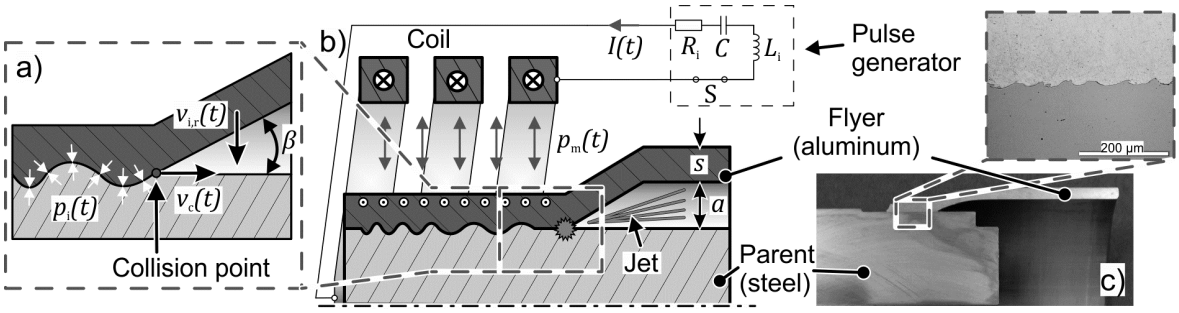


***Figure 1**: Magnetic pulse welding: a) Conditions at the collision zone, b) setup and principle, c) aluminum-steel joint, d) wavy interface. According to Lueg-Althoff et al., 2016*

For a successful solid state welding process, the atoms of the parts to be joined have to be brought into very close contact. Oxide layers and contaminants on real parts prevent this contact and have to be removed beforehand. In roll bonding or extrusion processes, the surface layers are cracked due to an intense surface enlargement. In impact welding processes, the surface cleaning and the removal of oxide layers is attributed to the jetting effect. The nature of this material flow, which is usually accompanied by a bright flash, is not completely understood yet, although it has been observed for both explosive welding (Bergmann et al., 1966) and MPW (Watanabe and Kumai, 2009).

In MPW of tubes, the first process step is usually the free electromagnetic compression (EMC). In this process stage, the flyer part is subjected to plastic strains, which might have an influence on the behavior of the surface layers. The compression of thin tubes is often inhomogeneous and accompanied by wrinkle formation, although inertia effects at high velocities are regarded as beneficial for a stable forming process, see e.g. Vivek et al. (2011). Geometrical and material inhomogeneities as well as the structural stiffness were identified as influencing factors for the formation of wrinkles in free EMC of aluminum tubes (Psyk et al., 2004). Demir et al. (2010) included the capability of predicting wrinkles during EMC into a numerical model. Besides dieless EMC, wrinkling was also considered for processes with die (Savadkoohian et al., 2017) and the design of electromagnetic form-closed joining processes (Park et al., 2005).

In this paper, the influence of the free EMC stage on the MPW process is analyzed regarding two parameters: the inhomogeneous forming behavior and the fragmentation and cracking of surface layers. Therefore, EMC experiments are performed in order to quantify the plastic strains by means of optical measurement technologies and digital image correlation. The adhesion of oxide layers on the tubes during the compression is analyzed by the help of artificial ceramic layers, which are easy to observe under the microscope. Numerical simulations help to identify the influencing factors on the wrinkle formation and the amount of plastic deformation. Finally, the influence of the free forming stage on the welding result is investigated in MPW experiments.

# 2 Experimental and Numerical Setup

EMC and MPW experiments were performed at two different pulse generators: A Maxwell Magneform Series 7000 with a maximum charging energy $E_{max}$ = 32 kJ and a Poynting SMU 0612 FS with $E_{max}$ = 9 kJ. The characteristics of the applied configurations at the two machines are listed in **Table 1**.

| | **Maxwell (*MW*) Magneform (Bank 2+3)** | **Poynting SMU 0612 FS (*SMU*)** |
|---|---|---|
| Max. charging energy $E_{max}$ | 12 kJ | 9 kJ |
| Max. charging voltage $U_{max}$ | 8.16 kV | 15 kV |
| Inner capacitance $C_i$ | 362 µF | 80 µF |
| Inner inductance $L_i$ | 78 nH | 73 nH |
| Inner resistance $R_i$ | 5.4 mΩ | 6.7 mΩ |
| Short circuit frequency $f$ | 29 kHz | 100 kHz |

***Table 1**: Characteristics of the applied pulse generator configurations*

The tube material was EN AW-6060, an aluminum alloy frequently used for automotive applications. From the as delivered T66 state, a heat treated (*ht*) state was achieved by soft-annealing at 500 °C for one hour and subsequent quenching at ambient air. In **Table 2** the material properties of this state are listed. The geometrical properties of the workpieces

and tools of the EMC setup are depicted in **Fig. 2**. The initial cross-sectional tube geometry was measured by a 3D scanner ATOS from GOM mbH. The final geometries were measured by a tactile coordinate measuring machine Zeiss PRISMO.

Two different EMC arrangements were compared in order to account for the different ways of performing MPW experiments. The compression of a tube's center can be used to create two separate weld seams in a two-front process, see e.g. Tamaki and Kojima (1988). On the contrary, the compression of a tube's end is applied for the creation of one-front MPW processes (see e.g. Bellmann et al., 2016). In the present study, a direct acting coil type K40-10/60 from Poynting GmbH was applied for EMC of the tube's center. This coil has ten turns over a working width of 60 mm. The forming of the tubes' ends was performed with a coil K97-8/90 in combination with a fieldshaper featuring an active zone width of 10 mm. The working length $l_w$ was set to 6 mm in this case. During the experiments, the discharge current $I(t)$ was measured using a Rogowski pickup coil CWR 9000 B from Power Electronic Measurements Ltd. The radial compression of the workpiece segments was recorded with a photonic Doppler velocimeter (PDV). For this purpose, a periscope style solution with beam deflection and PDV probes integrated into the fieldshaper were applied (see **Fig. 2a** and **c**), as presented in Lueg-Althoff et al. (2016).

| | |
|---|---|
| Young's modulus $E_y$ | 72 GPa |
| Tensile stress $R_m$ | 181 MPa |
| Flow stress $k_f$ | 80.6 MPa |
| Specific electrical conductivity $\kappa$ | 28.3 MS/m |

***Table 2**: Mechanical and electrical properties of the applied tube material (state ht)*

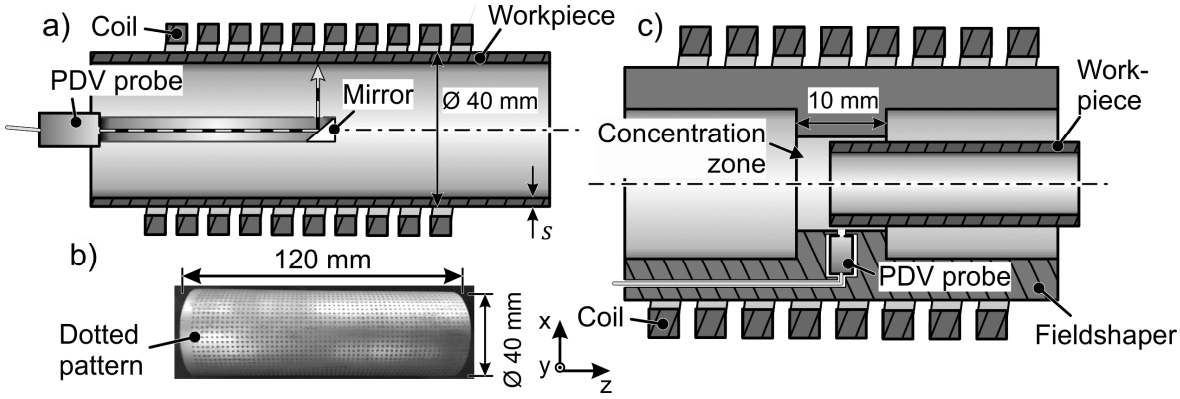


***Figure 2**: a) EMC of tube center with a direct acting coil, b) etched pattern on tube, c) EMC of tube end with a fieldshaper*

On selected workpieces, a pattern for strain analysis with the optical measurement system ARGUS from GOM mbH was applied by etching, see **Fig. 2b**. With Argus, the local plastic strains can be recorded and evaluated after the forming process (Höfling and Feldmann, 2002). On other tubes, oxide layers with a thickness of 15 µm, which are easily identifiable under the microscope, were applied by anodic oxidation to intensify the natural oxide layer. These specimens were investigated by light microscopy before and after the

experiments and the thickness and appearance of the layers was examined at the inner tube surfaces.

Numerical simulations were performed with LS-DYNA (version R 8.1). The measured coil current $I(t)$ and quasi-static flow curves obtained from tube tensile testing and extrapolated with the approach of Voce (Voce, 1948) as well as the measured initial tube geometries and the geometries of the coil windings served as input. The strain rate dependent behavior of the aluminum in both temper states was taken into account by using the Cowper-Symonds material model. The respective parameters of this model were determined as explained in Lorenz et al., 2016. By a numerical inverse material characterization approach, the values $C \approx 61{,}000$ and $p \approx 2.3$ were obtained.

# 3 Results and Discussion

The diagram in **Fig. 3** shows the results of different approaches for the determination of the strains during the EMC of the central areas of tubes by a direct acting coil at the SMU pulse generator. '*Exp.*' is the calculated strain based on the tactile measuring, '*ARGUS*' represents the result of the digital image correlation system (which could not be interpreted for all the experiments), '*LS-DYNA*' represents the local strains obtained from the numerical simulations, and '*Sim.*' summarizes the results based on the simulated maximum displacement. An increase of the discharge energy leads to an increase of the strains, whereas an increase of the tube wall thickness leads to lower strains. For the other pulse generator, similar tendencies exist.

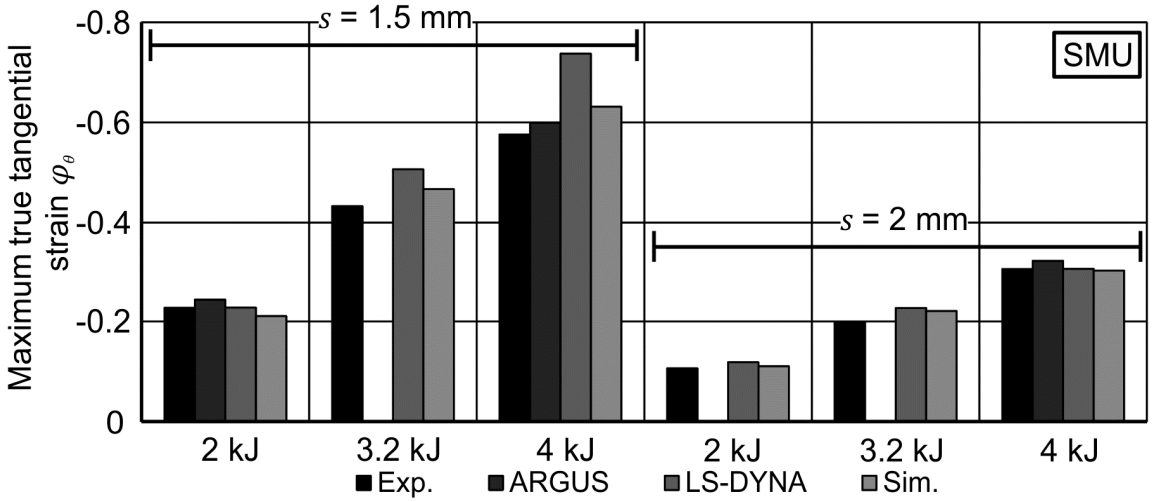


***Figure 3**: Obtained true strain depending on the discharge energy and the tube wall thickness: comparison of different analysis approaches*

It can be seen that the experimental and numerical results show only little deviations, so the simulation models are effective tools for process analysis. **Fig. 4a** shows the cross-sectional contours in the axial coil center of the inner surfaces of tubes with $s = 1.5$ mm after the EMC at $E = 4$ kJ. On the one hand, the nominal tube thickness was considered and

on the other hand, the measured initial cross-section area (i.e. the real wall thickness distribution) was integrated into the simulation models. Since the measured wall thickness was slightly higher than the nominal, the average final displacements were lower.

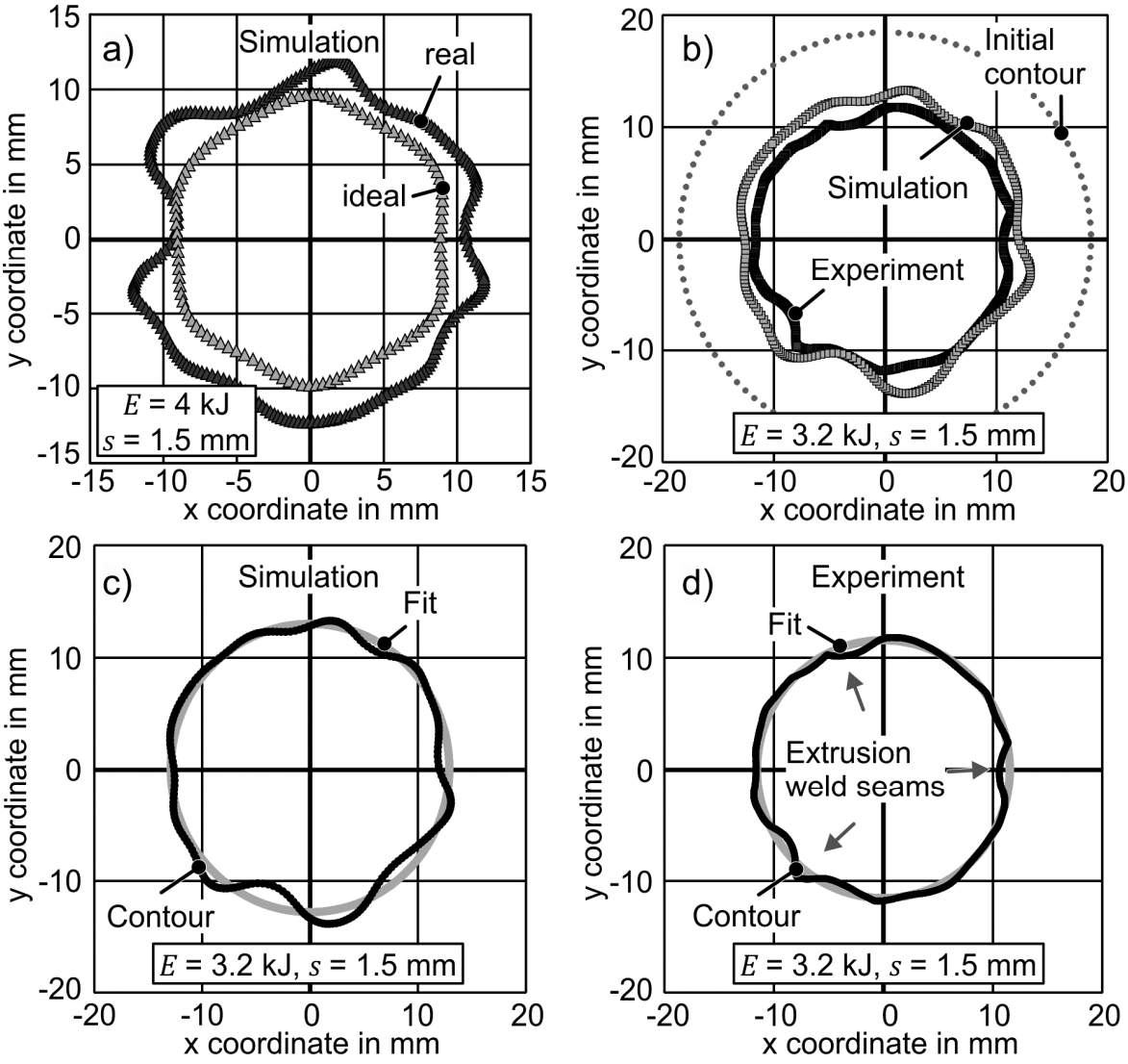


***Figure 4**: EMC of EN AW-6060 ht in the coil center at the SMU pulse generator. a) Influence of the wall thickness distribution, b) comparison of simulated and experimentally measured contour, c) comparison of simulated contour and circle fit, d) comparison of measured contour and circle fit*

Taking the real wall thicknesses into consideration leads to clear wrinkles around the circumference. At the same discharge energy, higher local strains and consequently pronounced wrinkles can be obtained at the SMU pulse generator, which features a much higher frequency of the discharge current compared to the Maxwell machine, see Table 1. For the ideal geometry, a slight hexagonal cross-section can be observed after EMC, see Fig. 4a. In **Fig. 4b**, a comparison between simulated and experimentally measured tube contours after EMC is presented. As mentioned before, the maximum compression can be

predicted accurately by the numerical model, the final contours are in acceptable agreement. In both experiment and simulation, wrinkling can be detected. However, the prediction of the positions and amplitudes of the wrinkles has room for further improvement.

Since different wall thicknesses around the circumference of the workpiece are one reason for the formation of wrinkles, a potential countermeasure against excessive wrinkling during EMC is the application of precise tubes with lower tolerances regarding variations of the wall thickness. Another important influencing factor can be found in the manufacturing process of the tube. Extrusion weld seams, which form during hot extrusion with porthole dies, usually feature finer grains and thus have different mechanical characteristics than the surrounding metal, see Psyk (2010). This leads to a different forming behavior during EMC and causes wrinkling, see **Fig. 4d**. In the numerical models, the position of the extrusion weld seams is not yet taken into account.

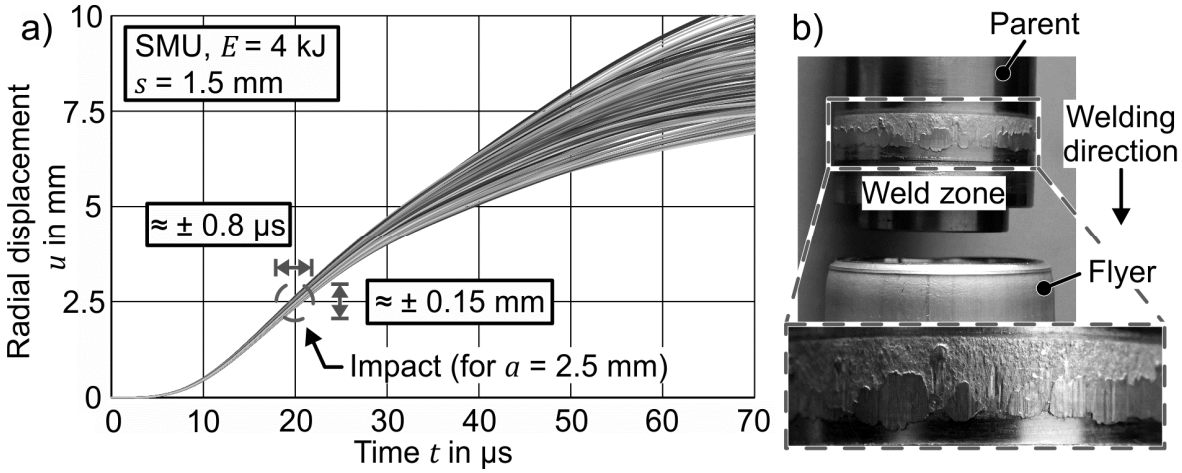


***Figure 5**: a) Simulated displacement of the nodes at the inner radius in the axial center of the tube, b) example MPW specimen after shear testing*

In **Fig. 5**, possible effects of the wrinkling during the EMC phase of an MPW process are shown. **Fig. 5a** summarizes the radial displacements of the nodes at the inner diameter at the axial center of the formed tube. Depending on their circumferential positions, the displacements differ due to the observed wrinkling. The series of curves fans out. A possible effect is that for initial standoffs typical of MPW (e.g., $a$ = 2.5 mm), the different areas of the flyer will impact the parent at different times. This may lead to different starting times of the welding effect and consequently to an irregular weld formation and varying weld lengths and qualities around the circumference, as shown in **Fig. 5b** for a single front MPW process.

The detrimental effects of wrinkling become more noticeable, the larger the standoff $a$ between flyer and parent is, see **Fig. 5a** and **Fig. 6c**. For experiments just below the welding limit, the flyer parts were axially cut (**Fig. 6a**), removed, and bent up (**Fig. 6b**) to expose their inner surfaces. At approx. the same radial impact velocities $v_{i,r} \approx 215$ m/s, the end of the impact zone is more ragged for a higher standoff $a$ = 2.5 mm. In case of MPW with direct acting single turn coils or multi turn coils with fieldshapers, the necessary axial slot in the coil or fieldshaper causes another intense discontinuity in the forming behavior.

In **Fig. 6d** it can be seen that the position of the slot in the fieldshaper is visible in the weld seam. At that position, the weld seam is shorter. The lower magnetic pressure near the slot reduces the forming velocity locally and thus causes wrinkling.

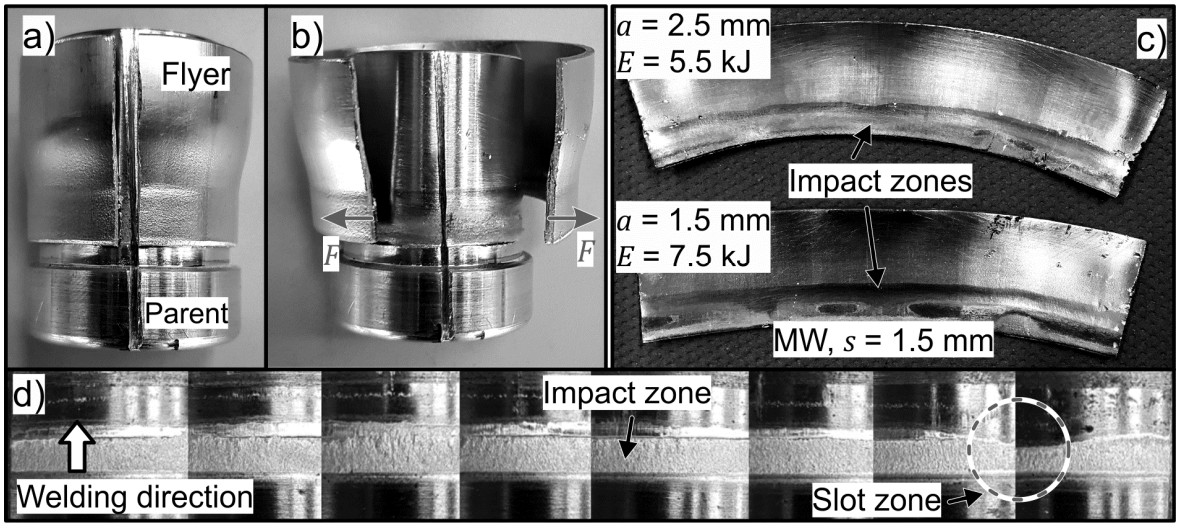


***Figure 6**: Influence of the initial standoff a on the appearance of the impact zone: a) axially cut specimen, b) bending of flyer, c) inner surface of flyer tubes after MPW experiments at conditions below the welding limit, d) composed view of the outer surface of a parent part after MPW and shear testing*

Besides the potential irregular weld formation, the strains caused by the EMC phase may also have a positive effect on the MPW process. **Fig. 7** shows microscopic images of artificial oxide ('Eloxal') layers with different initial thicknesses $s_{oxide}$ after EMC and MPW processes. It can be seen that already during the compression of the tube center clear cracks become visible in the oxide layer (**Fig. 7a** and **b**).

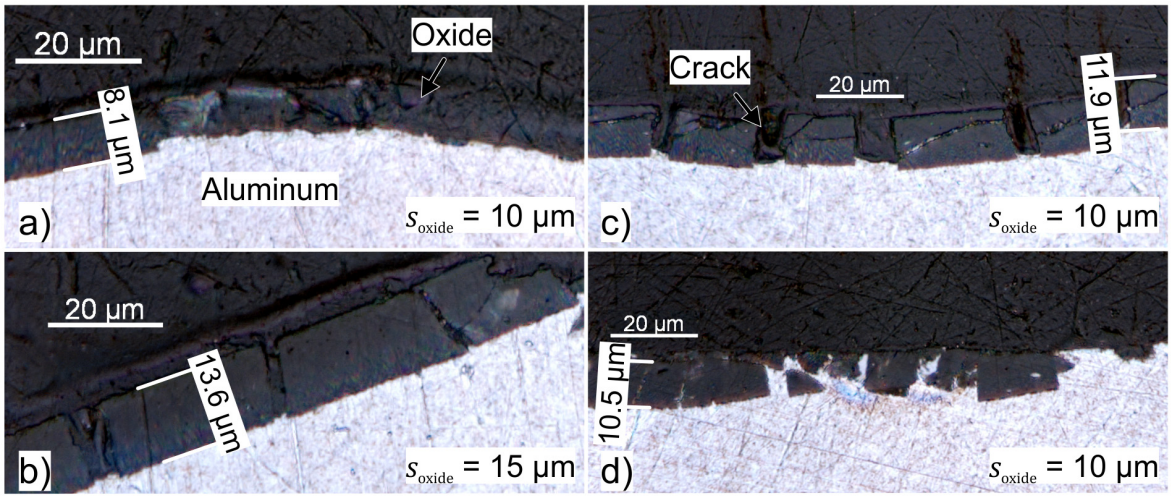


***Figure 7**: Fragmentation of artificial oxide layers in EMC and MPW: a) and b) EMC of the tube center, c) EMC of tube end, d) MPW process*

During a free compression of a tube end (**Fig. 7c**) even stronger fragmentation occurs, the width of the cracks increases. This fragmentation and cracking in the first process phase can support the jetting effect during the collision between flyer and parent even though the jetting was not able to remove the oxide layer completely in an exemplary single front MPW process, see **Fig. 7d**. No successful welding was obtained and the parent part is not displayed in this figure.

# 4 Conclusions and Outlook

MPW of tubular parts by EMC involves a free electromagnetic forming stage. In this process step, the flyer is accelerated up to the required impact velocity over the initial standoff. In this paper, the EMC stage was comprehensively investigated regarding its interactions with the weld formation by experimental and numerical means.

It was shown that the free compression could have significant effects on the welding process, which should be considered during process design:

- Wrinkles may occur due to geometrical, mechanical, manufacturing process, and tooling related inhomogeneities.
- Depending on the initial standoff $a$ between flyer and parent, these wrinkles lead to a non-uniform collision and welding process.
- The strains during the EMC can contribute to the cracking and fragmentation of surface layers, which may promote the cleaning by the jetting effect.

In order to minimize unwanted negative consequences resulting from the EMC, the following indications for process design can be given:

- The initial standoff $a$ between flyer and parent should be minimized.
- The geometry of the flyer should be as accurate as possible, especially regarding variations of the wall thickness. The position of the seam welds in extruded tubes should be taken into account. Tubes manufactured without the creation of seam welds are preferable.
- If a direct acting single turn coil or a fieldshaper are applied, the width of the axial slot should be small to limit the zone of reduced magnetic pressure.

In future experimental and numerical studies, the effectiveness of these countermeasures is to be analyzed. Moreover, existing analytical analysis frameworks of the EMC are to be expanded to predict the wrinkle formation without the need for elaborate numerical simulations.

# Acknowledgments

The presented results originate from research carried out within the subproject A1 of the priority program 1640 (“joining by plastic deformation”) funded by the German Research Foundation (DFG). The financial support is greatly acknowledged.

# References

Bellmann, J., Lueg-Althoff, J., Goebel, G., Gies, S., Beyer, E., Tekkaya, A. E., 2016. Effects of Surface Coatings on the Joint Formation During Magnetic Pulse Welding in Tube-to-Cylinder Configuration. In: Tekkaya, A.E., Kleiner, M. (Eds.), High Speed Forming 2016, Proc 7th Int Conf, Dortmund, Germany, pp. 279–288.

Bergmann, O. R., Cowan, G. R., Holtzman, A. H., 1966. Experimental evidence of jet formation during explosion cladding. Trans Met Soc of AIME 236, pp. 646-653.

Demir, O. K., Psyk, V., Tekkaya, A. E., 2010. Simulation of wrinkle formation in free electromagnetic tube compression. In: Babusci, K., Daehn, G.S., Marré, M., Tekkaya, A.E., Weddeling, C., Zhang, Y. (Eds.), High Speed Forming 2010, Proc 4th Int Conf, Columbus (OH), USA, pp. 181–188.

Höfling, R., Feldmann, P., 2002. Automatische Auswertung von Messrastern zur Dehnungsanalyse. tm-Technisches Messen 69 (10/2002). (in German)

Lorenz, A., Lueg-Althoff, J., Bellmann, J., Göbel, G., Gies, S., Weddeling, C., Beyer, E., Tekkaya, A. E., 2016. Workpiece Positioning during Magnetic Pulse Welding of Aluminum-Steel Joints. Welding J 95 (3), pp. 101–109.

Lueg-Althoff, J., Schilling, B., Bellmann, J., Gies, S., Schulze, S., Tekkaya, A. E., Beyer, E., 2016. Influence of the Wall Thicknesses on the Joint Quality During Magnetic Pulse Welding in Tube-to-Tube Configuration. In: Tekkaya, A.E., Kleiner, M. (Eds.), High Speed Forming 2016, Proc 7th Int Conf, Dortmund, Germany, pp. 259–268.

Mori, K.-i., Bay, N., Fratini, L., Micari, F., Tekkaya, A. E., 2013. Joining by plastic deformation. CIRP Annals - Manuf Technol 62 (2), pp. 673–694.

Park, Y.-B., Kim, H.-Y., Oh, S.-I., 2005. Design of axial/torque joint made by electromagnetic forming. Thin-Walled Structures 43 (5), pp. 826–844.

Psyk, V., Beerwald, C., Homberg, W., Kleiner, M., 2004. Electromagnetic Compression as Preforming Operation for Tubular Hydroforming Parts. In: Kleiner, M. (Ed.), High Speed Forming 2004, Proc 1st Int Conf, Dortmund, Germany, pp. 171–180.

Psyk, V., 2010. Prozesskette Krümmen – Elektromagnetisch Komprimieren – Innenhochdruckumformen für Rohre und profilförmige Bauteile, Dr.-Ing.-Dissertation, Dortmund. (in German)

Savadkoohian, H., Fallahi Arezoodar, A., Arezoo, B., 2017. Analytical and experimental study of wrinkling in electromagnetic tube compression. Int J Adv Manuf Technol 93, pp. 901–914.

Tamaki, K., Kojima, M., 1988. Factors affecting the result of electromagnetic welding of aluminum tube. Trans Japan Welding Soc 19 (1), pp. 53–59.

Vivek, A., Kim, K.-H., Daehn, G. S., 2011. Simulation and instrumentation of electromagnetic compression of steel tubes. J Mat Proc Technol 211 (5), pp. 840–850.

Voce, E., 1948. The relationship between stress and strain for homogeneous deformations. J Inst of Met 74, pp. 537–562.

Watanabe, M., Kumai, S., 2009. High-Speed Deformation and Collision Behavior of Pure Aluminum Plates in Magnetic Pulse Welding. Mat Trans 50 (8), pp. 2035–2042.